Received: 29 January 2024 | Revised: 3 July 2024 | Accepted: 9 July 2024

DOI: 10.1002/alz.14187

Alzheimer's & Dementia®
THE JOURNAL OF THE ALZHEIMER'S ASSOCIATION

RESEARCH ARTICLE

Cognitive resilience to Alzheimer's disease characterized by cell-type abundance

Nicholas O'Neill[1,2] | **Thor D. Stein**[3,4,5] | **Oluwatosin A. Olayinka**[1,2] | **Jenny A. Empawi**[2] | **Junming Hu**[1,2] | **Tong Tong**[1,2] | **Xiaoling Zhang**[1,2,6] | **Lindsay A. Farrer**[1,2,6,7,8,9]

[1]Bioinformatics Program, Boston University, Boston, Massachusetts, USA

[2]Department of Medicine (Section of Biomedical Genetics), Boston University Chobanian & Avedisian School of Medicine, Boston, Massachusetts, USA

[3]Department of Pathology and Laboratory Medicine, Boston University Chobanian & Avedisian School of Medicine, Boston, Massachusetts, USA

[4]VA Bedford Healthcare System, Bedford, Massachusetts, USA

[5]VA Boston Healthcare Center, Boston, Massachusetts, USA

[6]Department of Biostatistics, Boston University School of Public Health, Boston, Massachusetts, USA

[7]Department of Neurology, Boston University Chobanian & Avedisian School of Medicine, Boston, Massachusetts, USA

[8]Department of Ophthalmology, Boston University Chobanian & Avedisian School of Medicine, Boston, Massachusetts, USA

[9]Department of Epidemiology, Boston University School of Public Health, Boston, Massachusetts, USA

Correspondence
Xiaoling Zhang and Lindsay A. Farrer, Boston University School of Medicine, Biomedical Genetics E223, 72 East Concord Street, Boston, MA 02118, USA.
Email: zhangxl@bu.edu and farrer@bu.edu

Funding information
NIA, Grant/Award Numbers: P30AG10161, R01AG15819, R01AG17917, R01AG30146, R01AG36042, RC2AG036547, R01AG36836, R01AG48015, RF1AG57473, U01AG32984, U01AG46152, U01AG46161, U01AG61356, R01-AG048927, U01-AG058654, U54-AG052427, U19-AG068753, U01-AG062602, U01-AG072577, R01-AG080810; Illinois Department of Public Health; Translational Genomics Research Institute

Abstract

INTRODUCTION: The molecular basis of cognitive resilience (CR) among pathologically confirmed Alzheimer's disease (AD) cases is not well understood.

METHODS: Abundance of 13 cell types and neuronal subtypes in brain bulk RNA-seq data from the anterior caudate, dorsolateral prefrontal cortex (DLPFC), and posterior cingulate cortex (PCC) obtained from 434 AD cases, 318 cognitively resilient AD cases, and 188 controls in the Religious Orders Study and Rush Memory and Aging Project was estimated by deconvolution.

RESULTS: PVALB+ neuron abundance was negatively associated with cognitive status and tau pathology in the DLPFC and PCC ($P_{adj} < 0.001$) and the most reduced neuronal subtype in AD cases compared to controls in DLPFC ($P_{adj} = 8.4 \times 10^{-7}$) and PCC ($P_{adj} = 0.0015$). We identified genome-wide significant association of neuron abundance with *TMEM106B* single nucleotide polymorphism rs13237518 in PCC ($p = 6.08 \times 10^{-12}$). rs13237518 was also associated with amyloid beta ($p = 0.0085$) and tangles ($p = 0.0073$).

DISCUSSION: High abundance of PVALB+ neurons may be a marker of CR. *TMEM106B* variants may influence CR independent of AD pathology.

KEYWORDS
Alzheimer's disease, brain cell type abundance, cognitive resilience, deconvolution, PVALB, RNA sequencing, *TMEM106B*

Highlights

- Neuron retention and a lack of astrocytosis are highly predictive of Alzheimer's disease (AD) resilience.
- PVALB+ GABAergic and *RORB*+ glutamatergic neurons are associated with cognitive status.
- A *TMEM106B* single nucleotide polymorphism is related to lower AD risk, higher neuron count, and increased AD pathology.

1 | INTRODUCTION

Alzheimer's disease (AD) is characterized by amyloid beta (Aβ) deposition and tau aggregation, neuronal loss, and astrocytosis in the brain.[1,2] These cellular composition changes are associated with AD progression and cognitive impairment. For example, neuronal loss in the hippocampus is observed in the early stage of AD, indicating its role in causing early memory impairment.[3] In addition, ≈ 25% of cognitively normal individuals aged ≥ 75 exhibit AD-like neuropathology, including amyloid plaques, neurofibrillary tangles (NFTs), and neuronal loss in their brain autopsy,[4] which is defined as asymptomatic AD or apparent cognitive resilience (CR).[5–8] CR subjects have a lower frequency of comorbid neuropathology such as Lewy bodies, microinfarcts, and hippocampal sclerosis[8] and may be difficult to differentiate from those who would eventually exhibit cognitive decline in response to increasing AD pathology (i.e., preclinical AD). The quantification of the cellular population in aging brains provides insights into protective mechanisms against neurodegenerative diseases.

To quantify cell-type abundance within *post mortem* human brain samples, immunohistochemistry (IHC) assays targeting cell-type marker genes are commonly used.[9] Due to the nature of the assay, IHC is usually performed with a small number of antibodies, often one per cell type quantified,[9] and studies using IHC measurements are limited in sample size. Specific brain cell types identified by single-nuclei RNA sequencing (snRNA-seq) data generated from AD brains have been associated with disease progression.[10–13] Due to the complexity and current cost of snRNA-seq, deconvolution methods have been developed to quantify cell-type abundance from bulk RNA-seq data using reference genes that are manually selected,[14] derived from cell-sorted bulk RNA-seq,[15] or identified and weighted using single-cell or single-nuclei reference datasets.[16,17]

Cell-type abundance estimated from the deconvolution of bulk RNA-seq data from older adults can be used to characterize cellular change and enhance our understanding of cellular roles in healthy aging and AD. For example, Li et al. reported that decreased neuron and increased astrocyte proportions are associated with pathologically confirmed AD status, Braak staging, clinical dementia rating, and AD risk genetic variants.[18] Other researchers quantified the abundance of 33 cellular subtypes in deconvoluted bulk RNA-seq data derived from 638 Religious Orders Study and Rush Memory and Aging Project (ROSMAP) participant dorsolateral prefrontal cortex (DLPFC) samples and found the abundance of an inhibitory neuron subtype expressing somatostatin, SST, was strongly and inversely associated with tau protein level and cognitive decline.[19] Furthermore, multiple studies identified association of cell-fraction quantitative trait loci with genetic variants (i.e., cfQTLs), and integrated them with known disease loci to help reveal the underlying cellular mechanisms.[20,21] Li et al. deconvoluted the abundance of astrocytes, neurons, microglia, and oligodendrocytes in the ROSMAP, Mt. Sinai Brain Bank, and Genotype-Tissue Expression (GTEx) project datasets, and identified association of a *TMEM106B* frontotemporal lobar degeneration (FTLD)-protective variant, rs1990621, with increased neuronal proportion.[22]

In this study, we deconvoluted a comparatively large human bulk RNA-seq dataset comprising multiple regions of the same brain to characterize the abundance of six major brain cell types and eight neuron subtypes. This dataset includes 744 anterior caudate (AC), 1141 DLPFC, and 572 posterior cingulate cortex (PCC) samples obtained from subjects in the ROSMAP study. We reproducibly characterized cell-fraction changes and their associations with AD-related clinicopathological traits and then identified genetic drivers of these cell-fraction changes using matched whole genome sequencing (WGS) data by evaluating their association with AD risk variants and other phenotypes.

2 | METHODS

2.1 | Datasets and preprocessing

Two human prefrontal cortex (PFC) snRNA-seq reference datasets were downloaded and processed (Figure 1). One dataset, including 143,964 nuclei generated from 12 individuals with AD and 9 cognitively normal controls selected from the South West Dementia Brain Bank (SWDBB), was obtained from Gene Expression Omnibus (GEO; accession number GSE157827).[11] The second dataset, including 51,088 nuclei generated from 24 individuals with AD and 24 cognitively normal controls from the ROSMAP study, was obtained from Synapse (synapse ID: syn18485175).[10] The raw snRNA-seq count matrices were analyzed using Seurat toolkit version 3.1.2[23] as described previously.[24] Briefly, the expression values in both snRNA-seq datasets were normalized, scaled, dimensionally reduced to 10 principal components (PCs), and clustered using a k-nearest

RESEARCH IN CONTEXT

1. **Systematic review**: The authors reviewed the literature traditional (e.g., PubMed) as well as preprinted (e.g., medRxiv) sources on Alzheimer's disease (AD) cell-type abundance, neuron subtypes, cognitive resilience (CR), and *TMEM106B*.
2. **Interpretation**: We show that PVALB+ neuron abundance is associated with cognitive status and tau pathology in brain regions most vulnerable to AD. Astrocytes and oligodendrocytes were progressively more abundant in controls, cognitively resilient subjects with pathologically confirmed AD, and cognitively impaired AD cases, indicating that they may be a marker for CR. A *TMEM106B* variant that is associated with AD risk, amyloid beta level, and density of neurofibrillary tangles is also correlated with a reduction in neuron abundance.
3. **Future directions**: Follow-up studies should confirm these findings in larger cohorts. Future research should also examine the association of cell-type abundance with comorbid pathologies, as well as further characterize the relationship between cell type abundance and CR.

neighbor approach with a resolution of 0.8. The expression of marker genes for seven cell types (astrocytes, microglia, oligodendrocytes, oligodendrocyte precursor cells, endothelial cells, and GABAergic and glutamatergic neurons) was plotted against nuclei clusters. Clusters expressing only the marker genes of a single cell type were labeled and other clusters were separated, re-clustered, and again labeled according to cell-type markers. After cell typing, neurons accounted for 49.1% of cells in the SWDBB dataset and 60.4% of cells in the ROSMAP dataset. Because of the larger number of samples and higher proportion of neurons in the ROSMAP snRNA-seq dataset, we classified neurons into subtypes to increase understanding of the fate of different neurons in AD. Neurons were re-clustered to identify subtypes that are present in > 90% of subjects and express marker genes consistent with neuron subtypes characterized by Hodge et al.[25] Inhibitory neuron subtypes are identical to the conserved subtypes identified by Wang et al.[26]

Fastq files containing bulk RNA-seq data generated from 744 AC, 1141 DLPFC, and 572 PCC samples and AD-related clinical and pathological traits obtained from ROSMAP Study participants were downloaded from Synapse (synapse ID: syn23650893). Characteristics of these individuals are shown in Table 1. Data were preprocessed and analyzed using the TOPMed bulk RNA-seq pipeline (https://github.com/broadinstitute/gtex-pipeline/blob/master/TOPMed_RNAseq_pipeline.md). Briefly, fastq data quality was assessed using FastQC version 0.11.9, and reads were aligned to the human genome (GRCh38.103) using STAR version 2.7.5c and assigned to genes and quantified using RNA-SeQC version 2.3.6. RNA-SeQC read counts were used for further analyses.

TABLE 1 Number of samples per diagnosis and brain region.

Diagnosis	AC	DLPFC	PCC
AD	249 (196)	417 (274)	181 (133)
CR	217 (163)	294 (211)	154 (123)
CT	127 (104)	181 (130)	102 (76)
Total	723 (585)	1091 (796)	559 (430)

Note: Each sample has age, sex, and *post mortem* interval metadata. Numbers in parentheses indicate samples with matching WGS and TDP-43 pathology data.
Abbreviations: AC, anterior caudate; AD, pathologically confirmed Alzheimer's disease with dementia; CR, pathologically confirmed Alzheimer's disease without dementia, that is, cognitively resilient; CT, cognitively healthy control; DLPFC, dorsolateral prefrontal cortex; PCC, posterior cingulate cortex; TDP-43, TAR DNA-binding protein 43; WGS, whole genome sequencing.

2.2 | Deconvolution

Cell-type abundances were quantified within each bulk RNA-seq dataset using DeTREM deconvolution version 1.0.0,[24] an algorithm that uses human brain snRNA-seq reference data to deconvolute bulk RNA-seq while compensating for the differences between the technologies by reducing the impact of genes that are differentially captured by snRNA-seq compared to bulk RNA-seq. Bulk RNA-seq data were deconvoluted using the ROSMAP and SWDBB snRNA-seq datasets as reference. We used neuron subtype abundance measurements from deconvolution with the ROSMAP snRNA-seq reference dataset. The SWDBB snRNA-seq dataset, which has a higher number of glial cells and deeper coverage than the ROSMAP snRNA-seq dataset, was used as a reference for determining the abundance of glial cells. Samples missing seven or more cell types or cell subtypes were excluded. Neuron subtype abundance estimates were combined to quantify total neuron abundance.

2.3 | Cell-fraction association with AD status and AD-related traits

To associate cell-type abundance with AD traits we categorized subjects into three diagnoses by following the criteria recently published by Johnson et al.[5] Subjects with Consortium to Establish a Registry for Alzheimer's Disease scores indicating moderate or frequent neuritic plaques; a Braak stage of ≥ III; and evidence of cognitive impairment, defined as a Mini-Mental State Examination (MMSE) score < 24 or a diagnosis of cognitive impairment, were considered to have AD. Subjects with frequent neuritic plaques, a Braak stage of ≥ III, and no evidence of impairment were considered cognitively resilient (CR). This classification for CR is consistent with a suggested framework which decouples the effects of CR from the degree of neuropathologic damage.[27] Other subjects with no evidence of cognitive decline, possible or no neuritic plaques, and a Braak score of ≤ II were considered controls (CT). Those with a Braak score of III as well as no evidence of neuritic plaques or cognitive decline were also assigned to the CT

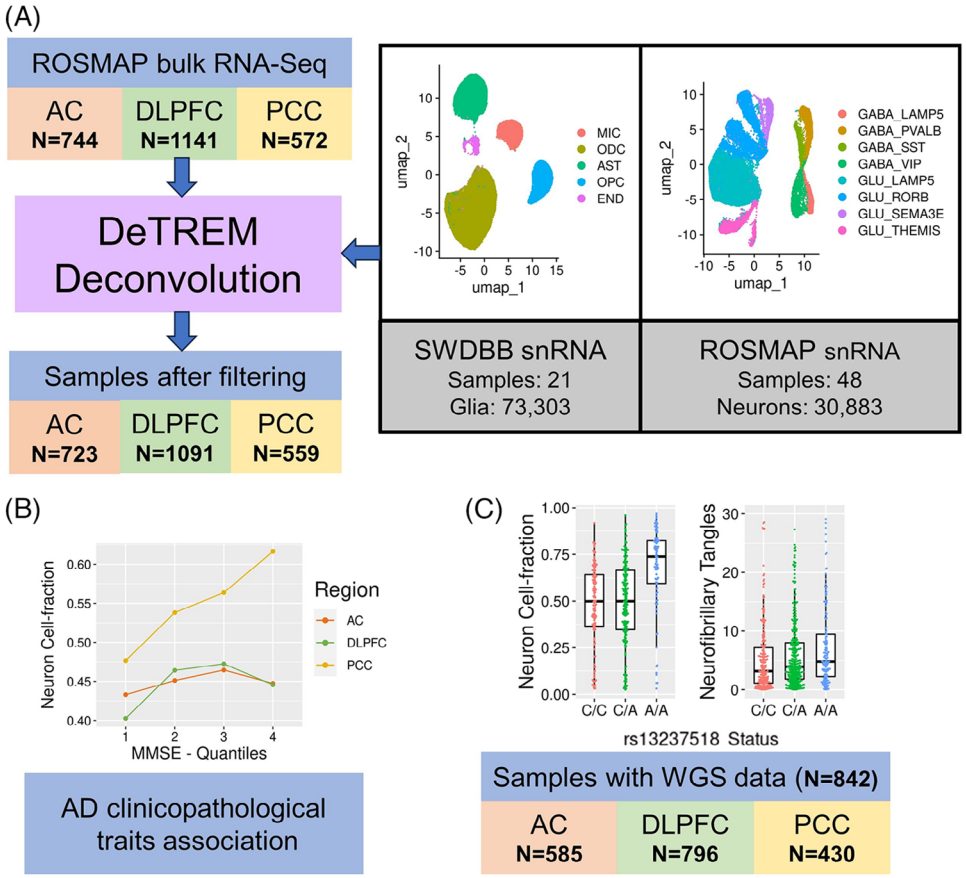

FIGURE 1 Overview of the study design. A, Cell fraction was calculated from 2457 bulk RNA-seq samples from among three brain regions (AC, DLPFC, PCC) in the ROSMAP cohort using the DeTREM algorithm. B, Cell fractions in the remaining samples were compared to diagnostic categories and clinicopathological traits. C, Cell-fraction quantitative trait locus analysis in samples with WGS data. AC, anterior caudate; AD, Alzheimer's disease; AST, astrocytes; DLPFC, dorsolateral prefrontal cortex; END, endothelial cells; MIC, microglia; ODC, oligodendrocytes; OPC, oligodendrocyte precursors; PCC, posterior cingulate cortex; ROSMAP, Religious Orders Study and Rush Memory and Aging Project; SWDBB, South West Dementia Brain Bank; WGS, whole genome sequencing.

group. The distribution of subjects according to diagnosis and brain region is shown in Table 1.

A generalized linear model in R (version 3.6.2) was applied to investigate the effect of cell fraction in each brain region on cognitive diagnosis by analyzing separately each pair of diagnoses (i.e., AD vs. CR, AD vs. CT, CR vs. CT) for each cell type and subtype. Models included covariates for cell fraction, age, sex, and *post mortem* interval (PMI). A second model investigated the relationship between cell fraction and each of three AD clinicopathological traits (Aβ burden and NFTs quantified by IHC,[28] and MMSE score) in each brain region and included covariates for cell fraction, age, sex, and PMI. Significance thresholds were determined using the Bonferroni method to correct for the number of cell fractions tested.

2.4 | Variance estimates

The variancePartition package (version 1.16.1) was used to verify that differences in cell-type abundance between diagnostic groups are generally reflected in the bulk RNA-seq expression values. Raw gene counts were normalized to 10,000 reads per subject for each bulk RNA-seq dataset. Genes with a normalized expression ≤ 1 and expression change < 20% between control and AD subjects in at least one brain region were excluded. The percentage of variance explained by each covariate was calculated using the following model, where group represents each pair of the three diagnostic groups:

$$\text{variance} \sim \text{age} + \text{sex} + \text{PMI} + (1|\text{group})$$

We ordered the genes by variance, removed genes whose overall variance is $< 1 \times 10^{-5}$, and binned the genes into 20 quantiles.

2.5 | cfQTL analysis

WGS data from 842 ROSMAP subjects were included in the Alzheimer's Disease Sequencing Project WGS release 3 (https://adsp.niagads.org/data/data-summary/) which were processed and joint-called by the Genome Center for Alzheimer's Disease (GCAD). Variants with minor allele count (MAC) < 5, not in

Hardy–Weinberg equilibrium ($P < 1.0 \times 10^{-6}$), or missing in > 10% of subjects were excluded. Subjects with > 10% missing genotypes were also removed. After quantity control filtering, 585 AC, 430 PCC, and 796 DLPFC bulk RNA-seq samples remained. A genome-wide association analysis was performed using the GENESIS package (version 2.16.1) to identify genetic variants associated with cell fraction (cfQTLs). Null models were generated for each cell type and brain region with cell fraction as outcome, and included a polygenic random effect; a genetic relationship matrix; and covariates for age, sex, and PMI. Subjects for whom a cell type was estimated to be absent were excluded from a model. The genetic inflation factor (lambda) for each model was calculated.

We tested an additional model including the same covariates to evaluate the impact of the number of *TMEM106B* rs13237518 *A* alleles, previously shown to be associated with neuron abundance[29] and FTLD,[30] on neuron subtype abundance in each brain region for which the subtype was present. Because of the association with FTLD, we added a term for the presence of TAR DNA-binding protein 43 (TDP-43) pathology extending beyond the amygdala.[28,31] Cell types and subtypes that were predicted to be absent in > 50% of subjects (missingness > 0.5) were excluded. We also tested the association of rs13237518 and AD pathology in 818 subjects with WGS and pathology measurements. PCC bulk RNA-seq samples were normalized to a total of 10,000 reads and *TMEM106B* expression was compared to rs13237518 status. Finally, we tested the association of established common AD risk variants (MAF > 0.15)[32] with cell-type abundance for each cell type and subtype per region with a missingness value < 0.75 using a model including covariates for age, sex, and PMI. Statistical significance was corrected for the number of cell fractions tested.

3 | RESULTS

3.1 | Non–subject-specific neuron subtypes

Using a clustering resolution of 0.1 and markers of four inhibitory/GABAergic neuron subtypes[25] we identified clusters expressing the genes *LAMP5*, *VIP*, *SST*, and *PVALB* (Figure S1 in supporting information). We followed the same procedure with glutamatergic/excitatory neurons with a resolution of 0.15 and identified a total of eight clusters expressing *LAMP5*, *THEMIS*, and *RORB* markers and a subtype specifically expressing *SEMA3E*, a gene related to neuronal development and layer formation,[25,33] which we condense to four subtypes (Figure S1). The relative abundance of each cell type and subtype for each subject in the ROSMAP snRNA-seq dataset is shown in Figure S2 in supporting information.

3.2 | Cell-type proportions are associated with cognitive status in multiple cortical regions

There were significant differences in the abundance of multiple cell types between cognitive states in two of the three cortical regions examined, most notably lower proportions of neurons in the DLPFC in AD cases compared to controls ($P_{adj} < 0.01$; Figure 2A). Conversely, AD cases had a significantly higher proportion of oligodendrocytes than controls in both DLPFC ($P_{adj} = 0.046$) and PCC ($P_{adj} = 0.0012$; Figure 2B). AD cases had significantly more astrocytes than CR cases in PCC ($P_{adj} = 0.047$) and controls in DLPFC ($P_{adj} < 0.05$). Among inhibitory neuron subtypes, the proportion of PVALB+ GABA neurons was lower in AD cases compared to controls in PCC ($P_{adj} = 0.0015$) and DLPFC ($P_{adj} = 8.39 \times 10^{-7}$). RORB+ GLU excitatory neurons were less abundant in AD cases compared to CR cases ($P_{adj} = 0.024$) and controls ($P_{adj} = 0.025$) in PCC (Figure 2B). In the DLPFC region, AD cases had a lower proportion of RORB+ GLU ($P_{adj} < 0.05$) and THEMIS+ GLU ($P_{adj} < 0.01$) neurons than controls (Figure 2A). As a sensitivity analysis, we estimated the correlation between the deconvoluted cell-type abundance and cell-type abundance measured by snRNA-seq among the samples common to our DLPFC bulk RNA-seq and the Mathys et al. snRNA-seq[10] datasets (Figure S3 in supporting information). We found that 10 of 14 (71%) of our deconvoluted cell-type proportions were correlated with proportions determined directly from snRNA-seq data ($-0.10 \leq r \leq 0.41$). The range of these correlation estimates was similar to that determined in a previous study ($-0.18 \leq r \leq 0.48$) which compared deconvoluted cell-type proportions to the same snRNA-seq dataset.[34] The finding of lower abundance of RORB+ GLU neurons in AD compared to CR cases was unchanged after adjusting for Aβ and was attenuated after adjusting for NFT burden (Figure S4A in supporting information).

3.3 | Gene expression variability among diagnostic groups

In both cortex DLPFC and PCC regions, the variation in gene expression was similar among AD cases compared to both CR cases and controls, but greater than the variation explained between CR cases and controls in the same regions (Figure 3). In contrast, there is relatively little variation in gene expression between the AD and CR groups in the caudate (AC) region. Gene expression variability between AD and control subjects was significantly greater in DLPFC compared to AC ($P = 3.6 \times 10^{-7}$), whereas this comparison between CR and CT subjects was not significant. These findings indicate that resiliency to clinical AD symptomatology explained by variation in gene expression is much greater in regions most vulnerable to AD.

3.4 | Association between cell fraction with AD related endophenotype traits

Analyses testing the association of deconvoluted cell-type fractions with AD related traits (Figure 4A) revealed that Aβ burden was significantly associated with neuron loss ($P_{adj} = 3.2 \times 10^{-4}$) and astrocytosis ($P_{adj} = 0.014$) in DLPFC but not in the other brain regions. This loss is accounted for primarily by PVALB+ GABA neurons ($P_{adj} = 0.022$).

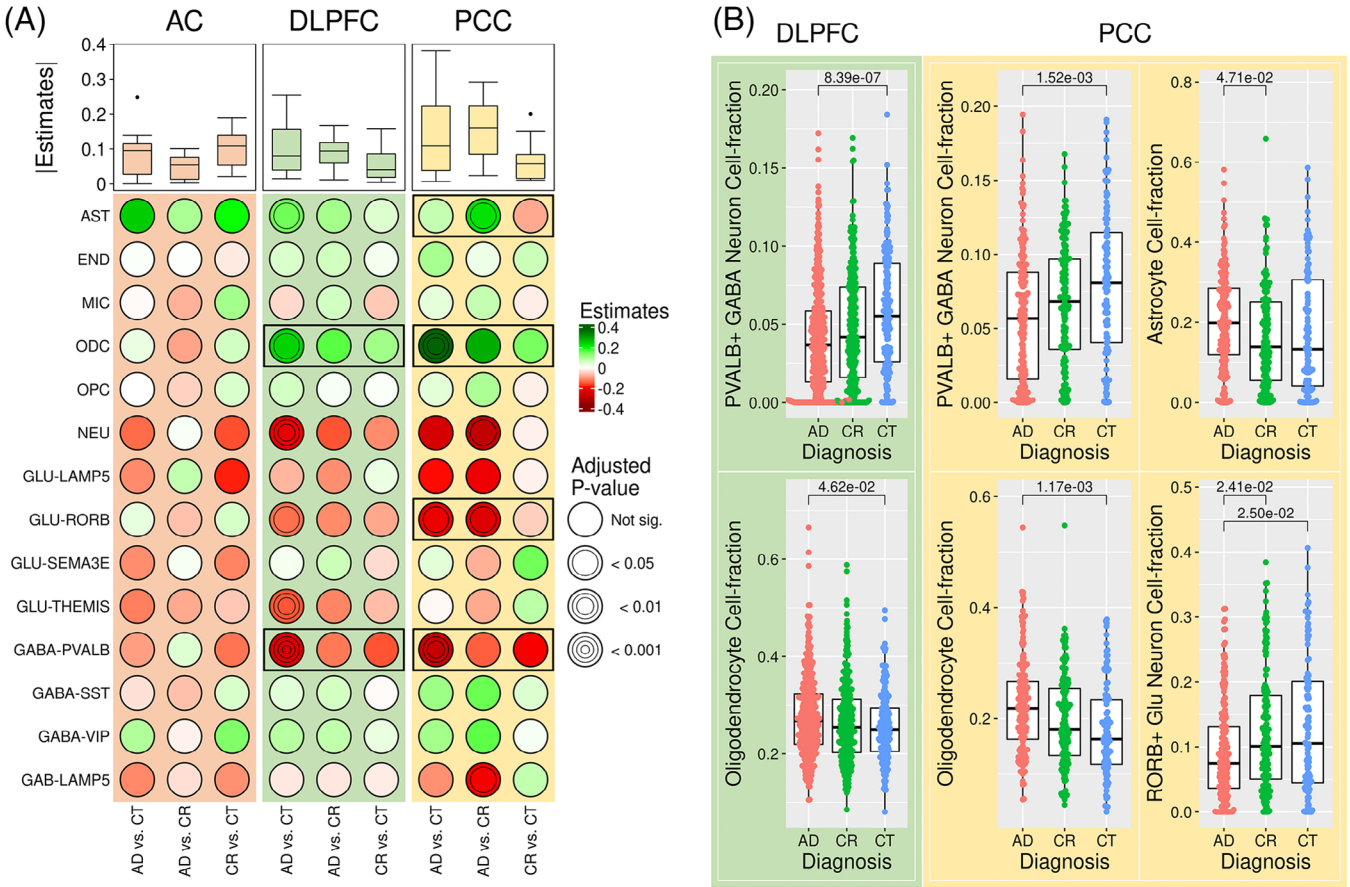

FIGURE 2 Deconvoluted cell-type proportions according to diagnosis in three brain regions. A, Association of diagnosis (AD = pathologically confirmed AD with dementia, CT = cognitively healthy control; CR = pathologically confirmed AD without dementia, i.e., cognitively resilient) with cell fraction (shown in row). Each circle shows the result for the comparison of the proportions of a cell type abundance between two diagnostic groups in one brain region. Effect size (β) and direction are indicated by color and the statistical significance is represented by concentric circles. A box plot of the absolute value of β from the combined 14 cell fractions is shown above each set of comparisons in the column. B, Box plots showing proportions of selected cell types in selected brain regions for each diagnostic group. AC, anterior caudate; AD, Alzheimer's disease; DLPFC, dorsolateral prefrontal cortex; PCC, posterior cingulate cortex.

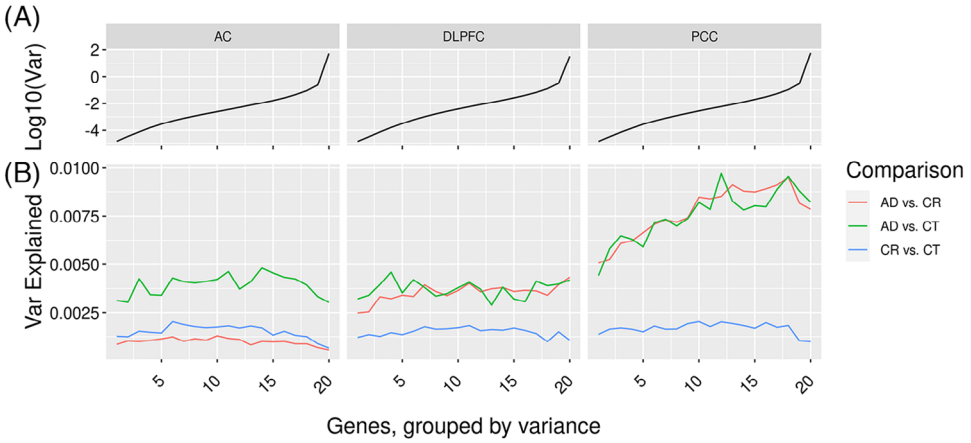

FIGURE 3 Gene expression variance explained by diagnostic group in each brain region. The variance in expression of each gene between pairs of diagnostic groups explained by AD status was calculated. After excluding genes with variance $<1 \times 10^{-5}$, the remaining genes were sorted by variance and grouped into 20 quantiles, shown on the *x* axis. A, Log of the overall variance of each gene quantile. B, Colored lines show the expression variance explained by the comparison of pairs of diagnoses for each quantile. AD, Alzheimer's disease; CR, cognitively resilient; CT, control.

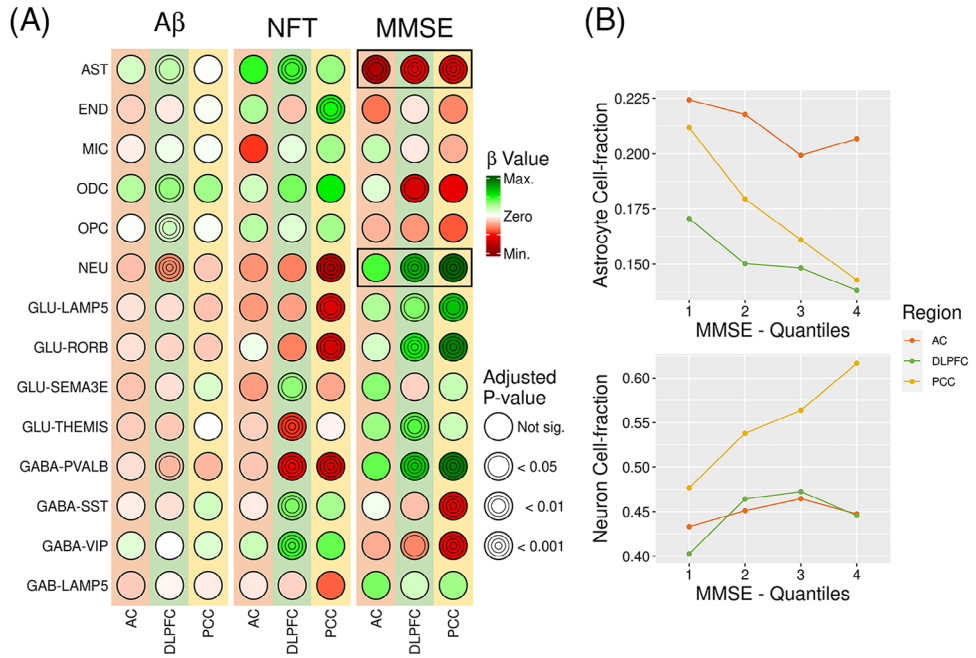

FIGURE 4 Association of deconvoluted cell proportions with brain measures of AD proteins and cognitive function. A, Results for Aβ, NFT, and MMSE score. Circles show the association for each cell type (row) and brain region (column). Effect size (β) and direction are shown according to color and statistical significance is denoted by concentric circles. The maximum and minimum β are 2 and −2 for Aβ, 4 and −4 for NFT, and 10 and −10 for MMSE score. B, MMSE scores were divided into quartiles and plotted against proportions of astrocytes and neurons. Lines are colored according to brain region. Aβ, amyloid beta; AC, anterior caudate; AD, Alzheimer's disease; DLPFC, dorsolateral prefrontal cortex; MMSE, Mini-Mental State Examination; NFT, neurofibrillary tangles; PCC, posterior cingulate cortex.

In contrast, NFT burden in the PCC was strongly associated with low abundance of neurons and several neuronal subtypes including LAMP5+ ($P_{adj} = 8.7 \times 10^{-3}$) and RORB+ ($P_{adj} = 1.5 \times 10^{-3}$) GLU neurons and PVALB+ GABA neurons ($P_{adj} = 3.8 \times 10^{-4}$). These associations were generally weaker in DLPFC for LAMP5+ ($P_{adj} = 0.40$) and RORB+ ($P_{adj} = 0.069$) GLU neurons, but PVALB+ GABA neurons (1.2×10^{-4}) remained the same and THEMIS+ GLU neurons are strongly associated with NFT severity only in DLPFC ($P_{adj} = 2.2 \times 10^{-4}$). NFT severity was also associated with abundance of SST+ GABA ($P_{adj} = 3.8 \times 10^{-3}$) and VIP+ GABA ($P_{adj} = 1.2 \times 10^{-5}$) neurons in the DLPFC.

Neuron abundance was significantly associated with MMSE score in DLPFC ($P_{adj} = 2.0 \times 10^{-5}$) and PCC ($P_{adj} = 3.3 \times 10^{-5}$; Figure 4B), and this relationship is accounted for primarily by excitatory neurons, particularly LAMP5+ GLU, RORB+ GLU, and THEMIS+ GLU. In contrast, SST+ GABA and VIP+ GABA excitatory neurons were negatively associated with MMSE in DLPFC and PCC ($P_{adj} < 0.001$; Figure 4A). Astrocyte abundance was inversely associated with MMSE score with a similar effect in all three brain regions. MMSE score was also associated with THEMIS+ GLU neurons in DFPLC but not in PCC, which is expected given that these neurons were not predicted to be abundant in PCC (Figure S5 in supporting information) and do not show significant associations with any AD-related traits in that region (Figure 4A). A sensitivity analysis to assess the impact of Aβ and NFT burden on the association of neuron abundance with MMSE score revealed that the abundance of astrocytes and neurons including RORB+ GLU and PVALB+ GAB in the DLPFC and PCC are still significantly associated with MMSE score (Figure S4B).

3.5 | Genome-wide association of neuron abundance QTLs

A genome-wide association study (GWAS) for neuron abundance conducted separately in each brain region revealed no evidence of genomic inflation in DLPFC ($\lambda = 1.01$, Figure S6A in supporting information) or PCC ($\lambda = 1.01$, Figure S6B). We identified one genome-wide significant (GWS) association with multiple variants in *TMEM106B* including an intronic 1 bp insertion (rs56761518; 7-12212493-G-GT) in the DLPFC GWAS ($\beta = 0.077$, $P = 5.13 \times 10^{-14}$, Figure 5A, Figure S6C) and rs4721064 located 1.4 kb downstream of *TMEM106B* in the PCC GWAS ($\beta = 0.071$, $Pp = 2.00 \times 10^{-9}$, Figure S6D). Association with this locus was previously reported in studies of other psychiatric disorders[22,29,35] and rs4721064 is only 505 bp away from and in high linkage disequilibrium (LD, $R^2 = 0.92$) with FTLD-protective variant rs1990621[22] (Figure S7 in supporting information). The *TMEM106B* rs13237518 *A* allele was previously reported to be associated with decreased AD risk at a GWS level[32] and is significantly associated with neuron cell fraction with the highest effect size in PCC ($\beta = 0.192$, $P = 1.71 \times 10^{-12}$). This association extends to several neuronal subtypes including LAMP5+ GABA and PVALB+ GABA inhibitory neurons and LAMP5+GLU and RORB+GLU excitatory neurons (Figure 5A,

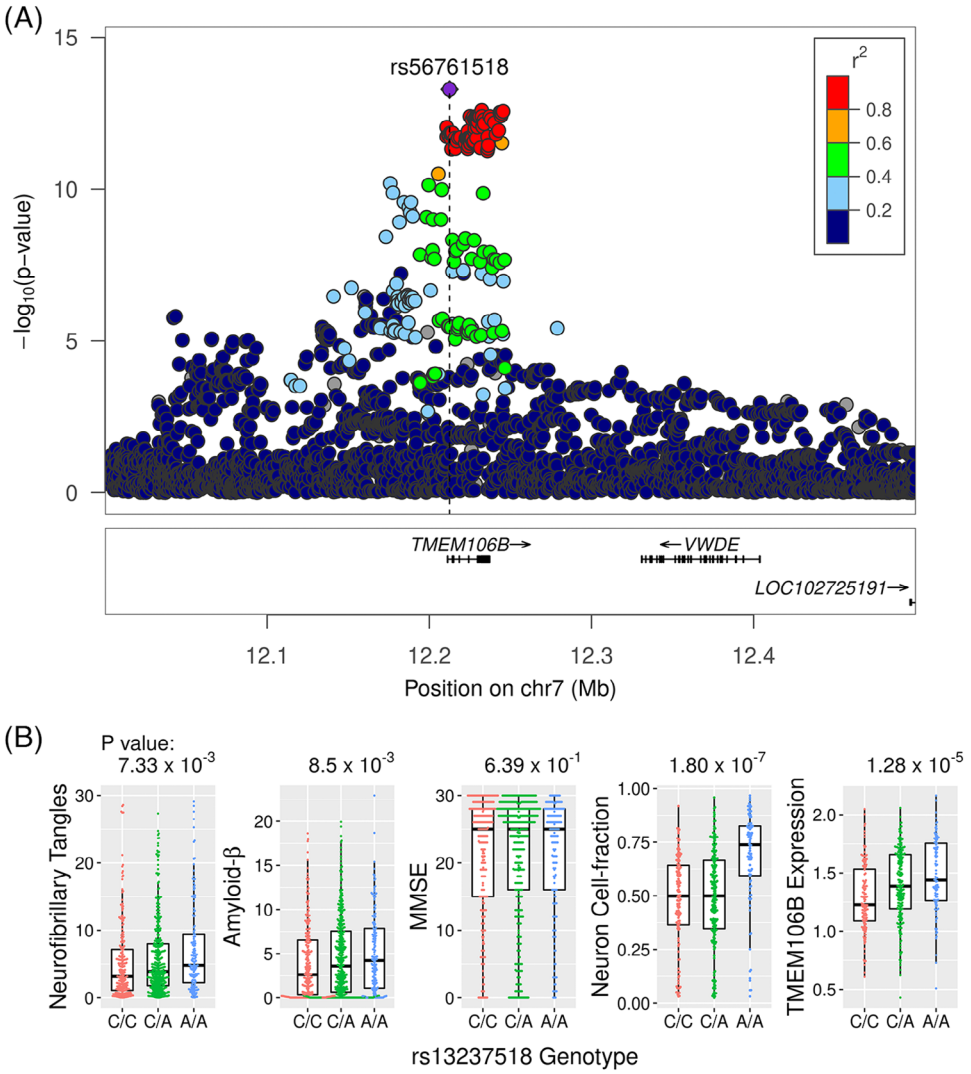

FIGURE 5 Association of *TMEM106B* with cell type QTLs. A, Locus zoom plot showing the association of neuron abundance in DLPFC with SNPs in the *TMEM106B* locus. Each dot represents one SNP, which is colored according to its correlation with the index SNP rs56761518. B, Box plots showing the association of rs13237518 with neurofibrillary tangles, amyloid beta, MMSE score, deconvoluted neuron cell fraction, and *TMEM106B* expression in PCC. DLPFC, dorsolateral prefrontal cortex; MMSE, Mini-Mental State Examination; PCC, posterior cingulate cortex; QTL, quantitative trait locus; SNP, single nucleotide polymorphism.

Table 2). rs13237518 was also significantly associated with each GLU neuron subtype (Table 2) and with increased neurofibrillary tangles ($P = 7.33 \times 10^{-3}$), Aβ pathology ($P = 8.5 \times 10^{-3}$), and *TMEM106B* expression in the PCC ($P = 1.28 \times 10^{-5}$; Figure 5B).

4 | DISCUSSION

4.1 | Brain cell-type abundance varies among cognitively impaired and resistant AD cases and controls

Although the number of large-scale snRNA-seq studies of AD is growing,[13,36–40] current costs and a high RNA-quality requirement indicate that deconvoluting more readily available bulk RNA-seq data is still valuable for generating cell-type or sub-cell type information, especially in less accessible tissues including the human brain. Previous deconvolution studies of AD-related cell-type abundance that were performed using relatively young cohorts[21] did not leverage cell-type signatures derived from snRNA-seq[18,22] focused on a single brain region,[19] or defined astrocyte and microglial cell subtypes that were apparently derived from few individuals.[19] In this study, we applied a recently developed method[24] to deconvolute bulk RNA-seq data obtained from ≈ 2500 ROSMAP Study samples. Unlike previous studies of cell-type abundance in AD, we investigated cell-type abundance changes specific for pathologically defined AD and CR by quantifying six major cell types and eight neuron subtypes in three brain regions including ones that are most directly and typically not affected by AD.

Consistent with previous studies,[18] we found that decreased neuron and increased astrocyte proportions are associated with pathologically confirmed AD. In particular, AD cases had a higher proportion of astrocytes than controls in DLPFC, whereas among those meeting

TABLE 2 Association of *TMEM106B* rs13237518 with estimated neuronal abundance by brain region.

	Anterior caudate				Dorsolateral prefrontal cortex				Posterior cingulate cortex			
Cell type	% Missing[a]	Beta	SE	P_{adj}	% Missing[a]	Beta	SE	P_{adj}	% Missing[a]	Beta	SE	P_{adj}
NEU	0	5.45E-02	1.06E-02	4.61E-06	0	6.61E-02	1.02E-02	2.24E-09	0	9.01E-02	1.55E-02	1.80E-07
GABA—LAMP5	5.2	1.81E-03	8.35E-04	0.4353	60.9	NA	NA	NA	17.5	5.09E-03	1.09E-03	6.07E-05
GABA—VIP	9.5	1.13E-04	1.06E-03	1	55.9	NA	NA	NA	35.6	−8.16E-04	1.44E-03	1
GABA—SST	31.8	6.37E-05	9.74E-04	1	75.7	NA	NA	NA	61	NA	NA	NA
GABA—PVALB	0.5	3.35E-03	1.11E-03	3.83E-02	5.9	6.48E-03	1.73E-03	2.75E-03	2.5	7.68E-03	3.08E-03	0.1829
GLU—THEMIS	48.3	5.99E-03	1.43E-03	4.40E-04	22.4	1.28E-02	3.11E-03	6.05E-04	55.6	NA	NA	NA
GLU—SEMA3E	10.4	1.04E-02	2.33E-03	1.50E-04	76.5	NA	NA	NA	14.1	7.51E-03	2.81E-03	0.1098
GLU—LAMP5	10.4	2.39E-02	6.61E-03	4.67E-03	10.1	2.40E-02	5.85E-03	6.46E-04	13.1	4.52E-02	8.66E-03	4.15E-06
GLU—RORB	12.2	9.00E-03	2.34E-03	1.90E-03	8.6	2.00E-02	4.96E-03	8.34E-04	4.4	2.32E-02	5.88E-03	1.33E-03

Abbreviations: GABA, inhibitory GABAergic neurons; GLU, excitatory glutamatergic neurons; NA, cell type excluded because missingness > 50%; NEU, total neurons; SE, standard error.
[a] Percent of samples for which cell type was predicted to be absent.

criteria for a pathological diagnosis of AD the astrocyte count in the PCC region was much higher in AD cases who were cognitively impaired or demented compared to those who were cognitively healthy prior to death. The fraction of oligodendrocytes (ODCs) was lowest in the controls and progressively higher in CR subjects and AD cases in both DLPFC and PCC regions. This finding suggests that ODC abundance might be a marker for CR. We also identified two neuronal subtypes, PVALB+ GABA and RORB+ GLU, that are significantly less abundant in AD cases compared to CT cases and controls in both DLPFC and PCC regions. These subtypes are significantly associated with lower performance on the MMSE and increased NFT count in the same regions. Our findings are consistent with a previous study showing that RORB may a marker of vulnerable neurons in AD[41] and suggest that preservation of RORB+ GLU neurons in the PCC is a potential marker of CR.

Our findings suggest that cognitive resiliency, based on relatively similar cell-type proportions between CR subjects and controls compared to AD cases in the PCC and DLPFC regions, is stronger in AD-vulnerable regions than in other regions (e.g., the AC). Although apparent CR is strongly related to a lack of comorbid neuropathology,[7,8] our diagnosis models did not consider neuropathological comorbidities. Adjusting for these comorbidities would reduce the CR effect whose cellular landscape we are characterizing. In addition, evidence of substantial loss of PVALB+ neurons in AD cases compared to control individuals in the PCC and DLPFC, and a much smaller reduction in CR individuals compared to AD cases, suggests that loss of these neurons may coincide with the processes leading to AD pathology rather than herald cognitive impairment. Of note, among neuron subtypes, PVALB+ GABA neurons were the most strongly associated with Aβ levels. Mice exposed to soluble Aβ displayed early dysfunction in PVALB+ neurons relative to excitatory neurons.[42,43] It has been suggested that PVALB+ neurons become hyperexcitable in early AD[42,44] and have an increase in energy demand because of their fast-spiking properties.[42,45] Other studies have found strong reductions in PVALB+ neurons in AD in humans and mice.[34,46] Progressive cognitive decline in persons with AD coincides with glutamatergic hypoactivation and is preceded by glutamatergic hyperactivation,[47] which has been observed in persons with mild cognitive impairment.[48] Additionally, resilience to AD pathology has been linked to strong preservation of neurons quantified by stereological measurements in the superior temporal sulcus.[6] Because the caudate is spared in persons with AD,[49] the lack of a resilience signature in the AC suggests that resilience is not characterized by general neuron abundance across the brain, but by reduction in neuronal loss in regions specifically vulnerable to AD.

4.2 | A *TMEM106B* variant is associated with reduced AD risk, increased AD pathology severity, and neuron abundance

The GWAS for cell-type abundance in regions affected by AD identified genome-wide significant associations with several variants in or near *TMEM106B*. Notably, we found that the rs13237518 *A* allele, which has

been associated with reduced risk of AD,[32] was associated with more severe AD pathology and greater neuron abundance. These apparently incongruent findings suggest that the protective effect of rs13237518 is mediated by maintenance of neurons rather than reduction of AD pathology. Future studies examining the relationship between *TMEM106B* and amyloid filaments[50] and tauopathy[51] are needed to validate this assertion. *TMEM106B* has been associated with the risk of other neurodegenerative diseases including FTLD[30,52,53] and limbic-predominant age-related TDP-43 encephalopathy.[54] *TMEM106B* regulates the size, localization, and activity of lysosomes[53,55,56] and mouse models have shown that deficiency of its encoded protein, transmembrane protein 106B, leads to lysosomal abnormalities and FTLD pathology.[56] Recently, the *TMEM106B* FTLD-protective variant rs1990621 that is in high LD with rs13237518, has been associated with increased neuronal proportion[22] and may play a role in resilience to age-related cognitive decline.[22,57]

4.3 | Study limitations

Our study has several limitations worth noting. Our focus on apparent CR[7] does not account for expected cognitive decline caused by comorbid pathologies and future studies should examine the effect of comorbid pathologies on cell-fraction change association with resilience. Related to this concern, our operational definition of CR, which is based on absence of cognitive impairment in the presence of AD pathology, does not consider the possibility that our association findings with cell-type proportions are related more to the severity of plaque and tangle burden than to CR. However, our sensitivity analyses demonstrated that severity of plaques did not impact the associations of RORB+ GLU neuron abundance with CR or MMSE score, and these associations were still significant but attenuated after adjustment for tangle severity. Another aspect of our study that should be considered is that measurements of cell-type abundance derived by deconvolution, IHC, or direct counting do not necessarily agree[24] and may lead to inconsistent results. In addition, differences in gene expression measured in snRNA-seq and bulk RNA-seq data may have inhibited our ability to accurately quantify some cellular activity. For example, microglia can be reprogrammed or recruited in response to stress but markers of microglia activity are not well captured by snRNA-seq.[58] The accuracy of these methods could be investigated further by future studies that quantify AD-related cell-type abundance in large snRNA-seq datasets, ideally spanning brain regions that are more or less affected by AD. Other studies found abundance of SST+ inhibitory neurons to be associated with reduced risk of AD,[34] tau accumulation, and cognitive decline in DLPFC,[13] findings which are consistent with those using protein measurement.[19] SST+ neuron loss in AD brains[13,34] was not replicated in our study, potentially due to our low call rate for SST+ GABA neurons in the DLPFC and PCC regions. We minimized the effect of low call rate on our results by limiting the number of cellular subtypes we quantified. This approach may also mitigate any issues caused by using a DLPFC snRNA-seq reference to deconvolute bulk RNA-seq data generated from two different brain regions, that is, PCC and AC. Additionally, the deconvolution method used in this study minimizes errors due to mis-specificity due to different tissue sources of the reference snRNA-seq and bulk RNA-seq datasets.[24] Finally, the snRNA-seq cell-type reference and ROSMAP bulk RNA-seq data were derived from primarily non-Hispanic White individuals. Because exposure to some AD risk factors and AD-related biological pathways (e.g., vascular disease, diabetes, low education, and others linked to diet, income, and occupation) disproportionally affect other diverse US populations including Black Americans and Hispanics, our results may not generalize to all populations.

5 | CONCLUSIONS

Our results suggest that abundance of astrocytes, ODCs, and PVALB+ GABAergic neurons may be markers of CR among persons with a pathological diagnosis of AD. We also identified several variants in *TMEM106B* that are associated with neuron abundance and, hence, may specifically influence resilience to cognitive decline but not AD pathology. Critically important for future studies is the identification and enumeration of disease associated glia subtypes, many of which can be difficult to investigate using deconvolution or snRNA-seq, as well as the characterization of comorbid pathologies and their relationship to cell-type abundance.

ACKNOWLEDGMENTS

The results published here are in whole or in part based on data obtained from the AD Knowledge Portal (https://adknowledgeportal.org). Study data were provided by the Rush Alzheimer's Disease Center, Rush University Medical Center, Chicago. Data collection was supported through funding by NIA grants P30AG10161 (ROS), R01AG15819 (ROSMAP; genomics and RNAseq), R01AG17917 (MAP), R01AG30146, R01AG36042 (5hC methylation, ATACseq), RC2AG036547 (H3K9A), R01AG36836 (RNAseq), R01AG48015 (monocyte RNAseq), RF1AG57473 (single nucleus RNAseq), U01AG32984 (genomic and whole exome sequencing), U01AG46152 (ROSMAP AMP-AD, targeted proteomics), U01AG46161 (TMT proteomics), U01AG61356 (whole genome sequencing, targeted proteomics, ROSMAP AMP-AD), the Illinois Department of Public Health (ROSMAP), and the Translational Genomics Research Institute (genomic). Additional phenotypic data can be requested at www.radc.rush.edu. This study was supported by National Institute on Aging grants R01-AG048927, U01-AG058654, U54-AG052427, U19-AG068753, U01-AG062602, U01-AG072577, and R01-AG080810.

CONFLICT OF INTEREST STATEMENT

L.A.F. received support from NIH grants and an honorarium for serving as a journal editor. None of the other authors have conflicts of interest to disclose. Author disclosures are available in the supporting information.

CONSENT STATEMENT

This study did not require informed consent because research participant data were obtained from public data repositories.

REFERENCES

1. Selkoe DJ, Hardy J. The amyloid hypothesis of Alzheimer's disease at 25 years. *EMBO Mol Med*. 2016;8(6):595-608.
2. Kinney JW, Bemiller SM, Murtishaw AS, Leisgang AM, Salazar AM, Lamb BT. Inflammation as a central mechanism in Alzheimer's disease. *Alzheimer's Dement Transl Res Clin Interv*. 2018;4:575-590.
3. Padurariu M, Ciobica A, Mavroudis I, Fotiou D, Baloyannis S. Hippocampal neuronal loss in the CA1 and CA3 areas of Alzheimer's disease patients. *Psychiatr Danub*. 2012;24(2):152-158.
4. Holtzman DM, Morris JC, Goate AM. Alzheimer's disease: the challenge of the second century. *Sci Transl Med*. 2011;3(77):77sr1.
5. Johnson ECB, Dammer EB, Duong DM, et al. Large-scale proteomic analysis of Alzheimer's disease brain and cerebrospinal fluid reveals early changes in energy metabolism associated with microglia and astrocyte activation. *Nat Med*. 2020;26(5):769-780.
6. Perez-Nievas BG, Stein TD, Tai HC, et al. Dissecting phenotypic traits linked to human resilience to Alzheimer's pathology. *Brain*. 2013;136(8):2510-2526.
7. Montine TJ, Cholerton BA, Corrada MM, et al. Concepts for brain aging: resistance, resilience, reserve, and compensation. *Alzheimer's Res Ther*. 2019;11(1):10-12.
8. Aiello Bowles EJ, Crane PK, Walker RL, et al. Cognitive Resilience to Alzheimer's Disease Pathology in the Human Brain. *J Alzheimer's Dis*. 2019;68(3):1071-1083.
9. Patrick E, Taga M, Ergun A, et al. Deconvolving the contributions of cell-type heterogeneity on cortical gene expression. *PLoS Comput Biol*. 2020;16(8):1-17.
10. Mathys H, Davila-Velderrain J, Peng Z, et al. Single-cell transcriptomic analysis of Alzheimer's disease. *Nature*. 2019;570(7761):332-337.
11. Lau SF, Cao H, Fu AKY, Ip NY. Single-nucleus transcriptome analysis reveals dysregulation of angiogenic endothelial cells and neuroprotective glia in Alzheimer's disease. *Proc Natl Acad Sci USA*. 2020;117(41):25800-25809.
12. Grubman A, Chew G, Ouyang J, et al. A single cell brain atlas in human Alzheimer's disease. *Nat Neurosci*. 2019;22(12):2087-2097.
13. Mathys H, Peng Z, Boix CA, et al. Single-cell atlas reveals correlates of high cognitive function, dementia, and resilience to Alzheimer's disease pathology. *Cell*. 2023;186(20):4365-4385. e27.
14. Kuhn A, Thu D, Waldvogel HJ, Faull RLM, Luthi-Carter R. Population-specific expression analysis (PSEA) reveals molecular changes in diseased brain. *Nat Methods*. 2011;8(11):945-947.
15. Newman AM, Liu CL, Green MR, et al. Robust enumeration of cell subsets from tissue expression profiles. *Nat Methods*. 2015;12(5):453-457.
16. Newman AM, Steen CB, Liu CL, et al. Determining cell type abundance and expression from bulk tissues with digital cytometry. *Nat Biotechnol*. 2019;37(7):773-782.
17. Wang X, Park J, Susztak K, Zhang NR, Li M. Bulk tissue cell type deconvolution with multi-subject single-cell expression reference. *Nat Commun*. 2019;10(1):380.
18. Li Z, Del-Aguila JL, Dube U, et al. Genetic variants associated with Alzheimer's disease confer different cerebral cortex cell-type population structure. *Genome Med*. 2018;10(1):1-19.
19. Cain A, Taga M, McCabe C, et al. Multi-cellular communities are perturbed in the aging human brain and with Alzheimer's disease. *bioRxiv*. 2020;4:5.
20. Wang D, Liu S, Warrell J, et al. Comprehensive functional genomic resource and integrative model for the human brain. *Science*. 2018;362(6420):eaat8464.
21. Donovan MKR, D'Antonio-Chronowska A, D'Antonio M, Frazer KA. Cellular deconvolution of GTEx tissues powers discovery of disease and cell-type associated regulatory variants. *Nat Commun*. 2020;11(1):1-14.
22. Li Z, Farias FHG, Dube U, et al. The TMEM106B FTLD-protective variant, rs1990621, is also associated with increased neuronal proportion. *Acta Neuropathol*. 2020;139(1):45-61.
23. Stuart T, Butler A, Hoffman P, et al. Comprehensive integration of single-cell data. *Cell*. 2019;177(7):1888-1902.
24. O'Neill NK, Stein TD, Hu J, et al. Bulk brain tissue cell - type deconvolution with bias correction for single - nuclei RNA sequencing data using DeTREM. *BMC Bioinformatics*. 2023:24(1):349.
25. Hodge RD, Bakken TE, Miller JA, et al. Conserved cell types with divergent features in human versus mouse cortex. *Nature*. 2019;573(7772):61-68.
26. Wang S, Ding P, Yuan J, et al. Integrative cross-species analysis of GABAergic neuron cell types and their functions in Alzheimer's disease. *Sci Rep*. 2022;12(1):1-12.
27. Phongpreecha T, Godrich D, Berson E, et al. Quantitative estimate of cognitive resilience and its medical and genetic associations. *Alzheimer's Res Ther*. 2023;15(1):1-12.
28. Klein HU, Trumpff C, Yang HS, et al. Characterization of mitochondrial DNA quantity and quality in the human aged and Alzheimer's disease brain. *Mol Neurodegener*. 2021;16(1):1-17.
29. Fujita M, Gao Z, Zeng L, et al. Cell-subtype specific effects of genetic variation in the aging and Alzheimer cortex. *Nat Genet*. 2024;56(4):605-614.
30. Van Deerlin VM, Sleiman PMA, Martinez-Lage M, et al. Common variants at 7p21 are associated with frontotemporal lobar degeneration with TDP-43 inclusions. *Nat Genet*. 2010;42(3):234-239.
31. Nag S, Yu L, Boyle PA, Leurgans SE, Bennett DA, Schneider JA. TDP-43 pathology in anterior temporal pole cortex in aging and Alzheimer's disease. *Acta Neuropathol Commun*. 2018;6(1):33.
32. Bellenguez C, Küçükali F, Jansen IE, et al. New insights into the genetic etiology of Alzheimer's disease and related dementias. *Nat Genet*. 2022;54(4):412-436.
33. Velona T, Altounian M, Roque M, et al. PlexinD1 and Sema3E determine laminar positioning of heterotopically projecting callosal neurons. *Mol Cell Neurosci*. 2019;100:103397.
34. Consens ME, Chen Y, Menon V, et al. Bulk and single-nucleus transcriptomics highlight intra-telencephalic and somatostatin neurons in Alzheimer's disease. *Front Mol Neurosci*. 2022;15:1-12.
35. Park Y, He L, Davila-Velderrain J, et al. Single-cell deconvolution of 3,000 post-mortem brain samples for eQTL and GWAS dissection in mental disorders. *bioRxiv*. 2021. 2021.01.21.426000.
36. Sun N, Victor MB, Park YP, et al. Human microglial state dynamics in Alzheimer's disease progression. *Cell*. 2023;186(20):4386-4403. e29.
37. Xiong X, James BT, Boix CA, et al. Single-cell epigenomic dissection of Alzheimer's disease pinpoints causal variants and reveals epigenome erosion. *Cell*. 2023;186(20):4422-4437. e21.
38. Green GS, Fujita M, Yang HS, et al. Cellular dynamics across aged human brains uncover a multicellular cascade leading to Alzheimer's disease. *bioRxiv*. 2023. 2023.03.07.531493.
39. Dileep V, Boix CA, Mathys H, et al. Neuronal DNA double-strand breaks lead to genome structural variations and 3D genome disruption in neurodegeneration. *Cell*. 2023;186(20):4404-4421. e20.
40. Gazestani V, Kamath T, Nadaf NM, et al. Early Alzheimer's disease pathology in human cortex involves transient cell states. *Cell*. 2023;186(20):4438-4453.
41. Leng K, Li E, Eser R, et al. Molecular characterization of selectively vulnerable neurons in Alzheimer's disease. *Nat Neurosci*. 2021;24(2):276-287.
42. Hijazi S, Smit AB, van Kesteren RE. Fast-spiking parvalbumin-positive interneurons in brain physiology and Alzheimer's disease. *Mol Psychiatry*. 2023;28(12):4954-4967.

43. Hijazi S, Heistek TS, van der Loo R, Mansvelder HD, Smit AB, van Kesteren RE. Hyperexcitable parvalbumin interneurons render hippocampal circuitry vulnerable to amyloid beta. *iScience*. 2020;23(7):101271.
44. Petrache AL, Rajulawalla A, Shi A, et al. Aberrant excitatory-inhibitory synaptic mechanisms in entorhinal cortex microcircuits during the pathogenesis of Alzheimer's disease. *Cereb Cortex*. 2019;29(4):1834-1850.
45. Hu H, Roth FC, Vandael D, Jonas P. Complementary tuning of Na+ and K+ channel gating underlies fast and energy-efficient action potentials in GABAergic interneuron axons. *Neuron*. 2018;98(1):156-165. e6.
46. Ali F, Baringer SL, Neal A, Choi EY, Kwan AC, Wirths O. Parvalbumin-positive neuron loss and amyloid-β deposits in the frontal cortex of Alzheimer's disease-related mice. *J Alzheimer's Dis*. 2019;72(4):1323-1339.
47. Findley CA, Bartke A, Hascup KN, Hascup ER. Amyloid beta-related alterations to glutamate signaling dynamics during Alzheimer's disease progression. *ASN Neuro*. 2019;11:1759091419855541.
48. Bell KFS, Bennett DA, Cuello AC. Paradoxical upregulation of glutamatergic presynaptic boutons during mild cognitive impairment. *J Neurosci*. 2007;27(40):10810-10817.
49. Persson K, Bohbot VD, Bogdanovic N, Selbæk G, Brækhus A, Engedal K. Finding of increased caudate nucleus in patients with Alzheimer's disease. *Acta Neurol Scand*. 2018;137(2):224-232.
50. Schweighauser M, Arseni D, Bacioglu M, et al. Age-dependent formation of TMEM106B amyloid filaments in human brains. *Nature*. 2022;605(7909):310-314.
51. Feng T, Du H, Yang C, Wang Y, Hu F. Loss of TMEM106B exacerbates Tau pathology and neurodegeneration in PS19 mice. *Acta Neuropathol*. 2024;147(1):62.
52. Van Der Zee J, Van Langenhove T, Kleinberger G, et al. TMEM106B is associated with frontotemporal lobar degeneration in a clinically diagnosed patient cohort. *Brain*. 2011;134(3):808-815.
53. Brady OA, Zheng Y, Murphy K, Huang M, Hu F. The frontotemporal lobar degeneration risk factor, TMEM106B, regulates lysosomal morphology and function. *Hum Mol Genet*. 2013;22(4):685-695.
54. Nelson PT, Dickson DW, Trojanowski JQ, et al. Limbic-predominant age-related TDP-43 encephalopathy (LATE): consensus working group report. *Brain*. 2019;142(6):1503-1527.
55. Stagi M, Klein ZA, Gould TJ, Bewersdorf J, Strittmatter SM. Lysosome size, motility and stress response regulated by fronto-temporal dementia modifier TMEM106B. *Mol Cell Neurosci*. 2014;61:226-240.
56. Feng T, Lacrampe A, Hu F. Physiological and pathological functions of TMEM106B: a gene associated with brain aging and multiple brain disorders. *Acta Neuropathol*. 2021;141(3):327-339.
57. White CC, Yang HS, Yu L, et al. Identification of genes associated with dissociation of cognitive performance and neuropathological burden: multistep analysis of genetic, epigenetic, and transcriptional data. *PLoS Med*. 2017;14(4):1-23.
58. Thrupp N, Sala Frigerio C, Wolfs L, et al. Single-nucleus RNA-Seq is not suitable for detection of microglial activation genes in humans. *Cell Rep*. 2020;32(13):108189.

SUPPORTING INFORMATION

Additional supporting information can be found online in the Supporting Information section at the end of this article.

How to cite this article: O'Neill N, Stein TD, Olayinka OA, et al. Cognitive resilience to Alzheimer's disease characterized by cell-type abundance. *Alzheimer's Dement*. 2024;20:6910–6921. https://doi.org/10.1002/alz.14187